

LARGE-EDDY SIMULATION OF A NOCTURNAL STRATOCUMULUS-TOPPED MARINE ATMOSPHERIC BOUNDARY LAYER: AN UNCERTAINTY ANALYSIS

ANDREAS CHLOND and ANDREAS WOLKAU*

Max-Planck-Institut für Meteorologie, Bundesstr. 55, 20146 Hamburg, Germany

(Received in final form 15 September 1999)

Abstract. A large-eddy simulation (LES) model has been used to study a nocturnal stratocumulus-topped marine atmospheric boundary layer. The main objectives of our study have been first to investigate the statistical significance of LES-derived data products. Second, to test the sensitivity of our LES results with respect to the representation of subgrid-scale mixing and microphysical processes, and third to evaluate and to quantify the parametric uncertainty arising from the incomplete knowledge of the environmental parameters that are required to specify the initial and boundary conditions of a particular case study. Model simulations were compared with observations obtained in solid stratocumulus during the third flight of the first 'Lagrangian' experiment of the Atlantic Stratocumulus Transition Experiment (ASTEX). Based on these simulations the following conclusions could be drawn. Resolution ($50 \times 50 \times 25 \text{ m}^3$) and domain size ($3.2 \times 3.2 \times 1.5 \text{ km}^3$) of the LES calculations were adequate from a numerical point of view to represent the essential features of the stratocumulus-topped boundary layer. However, the ensemble runs performed in our study to investigate the statistical significance of LES-derived data products demonstrate that the area-time averaging procedure for the second-order moments produces only a low degree of statistical reliability in the model results. This illustrates the necessity of having LES model results that are not only of adequate resolution but also of sufficiently large domain. The impact of different subgrid schemes was small, but the primary effects of drizzle were found to influence the boundary-layer structure in a climatologically significant way. The parametric uncertainty analysis revealed that the largest contribution to the variance of the LES-derived data products is due to the uncertainties in the cloud-top jump of total water mixing ratio and the net radiative forcing. The differences between the model and measurements for most of the simulated quantities were within the modelling uncertainties, but the calculated precipitation rate was found to differ significantly from that derived in the observations.

Keywords: Large-eddy simulation, Stratocumulus, Parametric uncertainty analysis, Drizzle.

1. Introduction

Low-level marine stratus clouds are important modulators of the earth's radiation budget. They increase the albedo compared to the underlying ocean surface but have little effect on the longwave radiation emitted to space. Consequently, satellite analyses of the top-of-the-atmosphere radiation budget show that areas affected by

* Current address: Warner Bros. Film Gmbh, Hans-Henry-Jahnn-Weg 35, 22303 Hamburg. (E-mail: chlond@dkrz.de)



these clouds can easily result in a net cloud forcing of -100 W m^{-2} and contribute substantially to a global net cloud forcing of about -17 W m^{-2} (Ramanathan et al., 1989; Harrison et al., 1990; Klein and Hartmann, 1993). In addition, modelling studies using a general circulation model with simplified parameterizations for cloud fraction and cloud microphysics (e.g., Slingo, 1990) indicate that modest changes in low cloud amount, cloud droplet size, or liquid water content could cause climatically significant changes to the global radiation budget. For these reasons, comprehensive field experiments and detailed modelling studies of the stratocumulus-topped marine boundary layer are of considerable importance to our understanding of the physics of the atmosphere, including possible effects of this boundary-layer regime on climate.

Models of the stratocumulus-topped boundary layer range in complexity from simple one-dimensional layer-averaged or mixed-layer models (Lilly, 1968; Deardorff, 1976; Schubert, 1976; Schubert et al., 1979a, b; Stage and Busingier, 1981a, b; Fravolo et al., 1981; Schaller and Kraus, 1981a, b; Hanson, 1984; Randall, 1984) to higher-ordered closure models (Oliver et al., 1978; Moeng and Arakawa, 1980; Moeng and Randall, 1984; Bougeault, 1985; Bougeault and André, 1986; Chen and Cotton, 1987; Duynkerke, 1989; Rogers and Koracin, 1992; Wang and Wang, 1994) and three-dimensional (3D) large-eddy simulation (LES) codes (Deardorff, 1980; Moeng, 1986; Moeng et al., 1992, 1995; Kogan et al., 1995), respectively. LES is now widely used in small-scale meteorology and is still one of the best techniques we have today for studying turbulence. The strength of LES lies in its explicit calculation of 3D time-evolving turbulent flow fields, which can be used to examine the time evolution of coherent structures and their contribution to turbulent transport. The major deficiency of LES models is that they are computationally demanding. They also generate large volumes of data, which require considerable analysis. Moreover, like most modelling techniques, LES-modelling is influenced by different uncertainties caused by modelling per se or by assumptions or uncertain values used in the model runs. Two main types of uncertainty affect our confidence in the results from numerical models: parametric uncertainty and structural uncertainty. Parametric uncertainty arise because of incomplete knowledge of model parameters such as empirical quantities, defined constants, and boundary conditions. Structural uncertainty in models arises because of inaccurate treatment of dynamical and physical processes, inexact numerical schemes, inadequate resolutions, and limited domain sizes. In general, the total uncertainty in modelling depends on these factors in a complicated and often counterintuitive way (Tatang, 1997).

In this paper we study three related aspects of LES in the stratocumulus-topped boundary layer. Our study focuses on some aspects of parametric and structural uncertainty and includes the following items:

1. We investigate the statistical significance of LES-derived data products. This has been done by performing ensemble runs of the stratocumulus-topped

boundary layer to demonstrate the stochastic nature of the turbulent processes within the boundary layer.

2. We examine the sensitivity of our LES-model with respect to the treatment of subgrid-scale processes and microphysical processes. For this purpose we have started model runs using Deardorff's and Schumann's parameterization scheme, respectively. Likewise, we investigate the sensitivity of model results in response to Kessler's and Lüpkes' drizzle parameterization scheme, respectively, and by deactivation of all precipitation processes.
3. We examine the sensitivity of our LES results with respect to the assumed values of various external, environmental conditions. Moreover, we apply a methodology for objective determination of the uncertainty in LES-derived quantities. The methodology is based on standard error-propagation procedures and yields expressions for probable errors as a function of the relevant parameters.

The paper is organized as follows. In Section 2 a brief overview of our LES-model is given. The design of the numerical simulation is described in Section 3, and the simulation results are presented and discussed in Section 4. Finally, summary and conclusions are given in Section 5.

2. Model Description

The basic dynamical framework employed is a modified and upgraded version of a model described in Chlond (1992, 1994) and Müller and Chlond (1996). The general idea focuses on the LES concept; that is, the model explicitly calculates the spatial averages, which hopefully represent the dominant large-scale motions, while parameterizing the effect of the small scales on the averaged flow quantities. The model uses Boussinesq-equations for the components of velocity u , v , w , liquid water potential temperature θ_1 and total water content q . These equations are formulated in a Cartesian coordinate system that is translated with the geostrophic wind to follow a trajectory of air in a Lagrangian manner. In that way, the marine stratocumulus case is treated as a time-dependent, quasi-local development. The model includes most of the physical processes occurring in the moist boundary layer. It takes into account infrared radiative cooling in cloudy conditions (using a simple effective emissivity-like approach) and the influence of large-scale vertical motions. The subgrid-scale (SGS) model is based on a transport equation for the SGS turbulent energy. To represent SGS fluxes two different closure schemes could be used: either the parameterization scheme of Deardorff (Deardorff, 1980) or the parameterization scheme of Schumann (Schumann, 1991). The schemes differ in that Schumann's scheme applies the limiting effect of stable stratification only to the length-scales for SGS effects of vertical eddy diffusivities of heat and scalars but not to those of momentum. In contrast, Deardorff (1980) proposed to reduce all the length scales for stable stratification. To take into account the microphysical

processes we have implemented two different bulk parameterization schemes into our LES-model: Kessler's parameterization scheme (Kessler, 1969) and Lüpkes' variable parameterization scheme (Lüpkes, 1991). Both schemes utilize a partitioning of total liquid water into two species with separated predictive equations: cloud water, which is assumed to move with the air, and rain water, which falls through the air. The parameterized microphysical processes include condensation, evaporation, coalescence and sedimentation. These conversion mechanisms are parameterized in terms of resolved scale variables such as mass and number densities of water species. The main difference between both schemes is that Lüpkes' scheme considers an additional quantity, besides the cloud water and rain water content, to characterize a droplet spectrum, namely, the rain droplet number density.

The solution of the basic equations is based on a finite differencing method on an equidistant grid. Cyclic lateral boundary conditions were applied and a Rayleigh damping layer in the upper third of the domain was utilized to absorb vertically propagating gravity waves. At the lower boundary prescribed fluxes of momentum, heat and moisture were imposed. Advection of momentum is formulated using a second-order scheme that conserves the integral of linear and quadratic quantities up to very small errors (Piacsek and Williams, 1970). For scalars a monotone advection algorithm is applied (Chlond, 1994). The time integration scheme utilizes the Adams-Bashforth scheme and the Euler scheme. Pressure is determined diagnostically by the solution of a Poisson equation using a Fast-Fourier-Transformation method (horizontal) and a finite-differencing method (vertical). The ensemble runs, and the runs that utilize different microphysical and subgrid-scale models, use a computational domain of size $3.2 \times 3.2 \times 1.5 \text{ km}^3$. The sensitivity runs have been performed in a larger domain ($28.8 \times 3.2 \times 1.5 \text{ km}^3$) in order to enhance the signal-to-noise ratio. The grid intervals are fixed to $\Delta x = \Delta y = 50 \text{ m}$ and $\Delta z = 25 \text{ m}$. A time step of 3 s was used for all runs.

3. Model Initialization and Forcing

In this paper the LES model is tested against observations of the structure of the marine stratocumulus layer observed during the first Lagrangian (Albrecht et al., 1995) experiment of the Atlantic Stratocumulus Transition Experiment (ASTEX). More specifically, the case is based on flight RF06 of the National Center for Atmospheric Research's Electra in the night and early morning of 13 June 1992 at about 37° N , 24° W . This data set is extensively described by de Roode and Duynkerke (1997) and Duynkerke et al. (1999), so only a short summary is given here.

The case study was of stratocumulus cloud cover over the North Atlantic that was in a transition stage, changing from a horizontally homogeneous cloud layer to a decoupled boundary layer with cumulus penetrating the stratocumulus deck

from below. Observations are made by seven research aircraft, from a research ship and from the islands of Santa Maria (Azores) and Porto Santo (Madeira). Aircraft flights were made at different levels above, within and below the stratocumulus deck. The navigation was such that the aircraft remained roughly in the same air mass, and the microphysical, radiative and turbulence measurements were made at heights between 30 m and 2800 m. The data were considered suitable for preparing initial and boundary conditions for a 4-hour model simulation of the evolution of the boundary layer, commencing at 0700 UTC on 13 June 1992.

The initial conditions for the model have been chosen such as to be essentially consistent with the conditions met during the observations and were specified in the form of simplified vertical profiles of the two horizontal wind components, the liquid-water potential temperature, and the total water content according to:

$$(\bar{u}, \bar{v})[\text{m s}^{-1}] = \begin{cases} (-1.7, -10) & 0 < z \leq -662.5 \text{ m} \\ (-1.7 - 0.026(z - 662.5), -10) & 662.5 < z \leq 712.5 \text{ m} \\ (-3.0, -10) & 712.5 < z \leq 1500 \text{ m} \end{cases} \quad (1)$$

$$\bar{\theta}_l [\text{K}] = \begin{cases} 288.0 & 0 < z \leq 662.5 \text{ m} \\ 288.0 + 0.11(z - 662.5) & 662.5 < z \leq 712.5 \text{ m} \\ 293.5 + 6 \times 10^{-3}(z - 712.5) & 712.5 < z < 1500 \text{ m} \end{cases} \quad (2)$$

$$\bar{q}[\text{g kg}^{-1}] = \begin{cases} 10.7 & 0 < z \leq 662.5 \text{ m} \\ 10.7 - 0.032(z - 662.5) & 662.5 < z \leq 712.5 \text{ m} \\ 9.1 - 2.4 \times 10^{-3}(z - 712.5) & 712.5 < z \leq 1500 \text{ m} \end{cases} \quad (3)$$

Thus, the profiles were independent of height below the base of the inversion (at $z = 662.5$ m), and varied linearly with height between the base and the top of the inversion at cloud top, and above the cloud, with jumps of $(\Delta\bar{q})_{\text{inv}} = -1.6 \text{ g kg}^{-1}$ and $(\Delta\bar{\theta})_{\text{inv}} = 5.5 \text{ K}$ in the liquid-water potential temperature and the total water content across the inversion, respectively. Cloud base was at $z = 312.5$ m and cloud top at $z = 712.5$ m. A uniform geostrophic wind was assumed $(u_g, v_g) = (-3, -10) \text{ m s}^{-1}$, and an initial value for subgrid turbulent kinetic energy of $1 \text{ m}^2 \text{ s}^{-2}$ was specified for $z < 687.5$ m. The fluxes of momentum heat and moisture fluxes at the surface were prescribed as:

$$\overline{(\bar{u}'w', \bar{v}'w')} = -(\bar{u}(\Delta z/2), \bar{v}(\Delta z/2)) \cdot u_*^2 / (\bar{u}^2(\Delta z/2) + \bar{v}^2(\Delta z/2))^{1/2}, \quad (4)$$

$$\overline{w'\theta'} = 1.3 \times 10^{-2} \text{ K m s}^{-1}, \quad (5)$$

$$\overline{w'q'_v} = 1.8 \times 10^{-5} \text{ kg m s}^{-1} \text{ kg}^{-1}, \quad (6)$$

where the friction velocity is fixed to $u_* = 0.3 \text{ m s}^{-1}$.

The net longwave radiation parameterization was a prescribed function of the liquid-water path (the net shortwave radiation was assumed to be zero) and is parameterized as:

$$F_{\text{NET}}(z) = F_{\text{NET}}^{\text{CT}} \cdot \exp(-a \cdot \text{LWP}(z, z_{\text{TOP}})), \quad (7)$$

where $F_{\text{NET}}^{\text{CT}} = 74 \text{ W m}^{-2}$ is the net longwave cooling at cloud top, $a = 136 \text{ m}^2 \text{ kg}^{-1}$ is a constant, and $\text{LWP}(z, z_{\text{TOP}})$ denotes the liquid water path between z and the top of the model domain z_{TOP} .

The Coriolis parameter is set to $f = 8.7 \times 10^{-5} \text{ s}^{-1}$ corresponding to a latitude of about 36.6° N) and the surface pressure is $p_{00} = 1028.8 \text{ hPa}$. The large-scale divergence was set to $1.5 \times 10^{-5} \text{ s}^{-1}$, resulting in a profile for the large-scale subsidence according to: $w_{\text{LS}} = 1.5 \times 10^{-5} z \text{ m s}^{-1}$, for z in m. All initial profiles were assumed to be horizontally homogeneous, except for the temperature field. In order to start the convective instability, spatially uncorrelated random perturbations, uniformly distributed between -0.1 K and 0.1 K , were applied to the initial temperature field at all grid points with $z < 687.5 \text{ m}$. This specification of model initialization and forcing has also been used in the European Cloud-Resolving Modelling (EUCREM) intercomparison project where the main focus has been on the entrainment velocity, which is the most important parameter for the cloud development (Duykerke et al., 1999).

4. Results

4.1. STATISTICAL SIGNIFICANCE OF LES RESULTS

A source of uncertainty in LES modelling emerges from the fact that the statistical characteristics used to describe the structure and dynamics of the boundary layer are computed in the form of spatial/temporal averages from one realization of the process over a record of finite length. Boundary-layer flows are turbulent and as such deterministic, in the sense that they can be described by an explicit mathematical relationship (i.e., the Navier-Stokes or Boussinesq equations), however, they exhibit random behaviour. Therefore, the complex nature of turbulence inevitably forces us to deal with the fundamental concepts related to the averaging process. The statistical average in LES modelling studies is taken as spatial/temporal average over a record of finite length. This contrasts with theoretical studies in turbulence that operate with ensemble averages, where the average is taken over a infinite number of realizations. Fortunately, ergodic theory tells us that ensemble averages can be approximated by the averages taken over sufficiently large time or space intervals if the stochastic process is stationary (in time) or homogeneous (in space) (e.g., Monin and Yaglom, 1971).

The averaging problem has always been of great concern among atmospheric scientists. The key question that arose in this connection was: How rapidly do the various temporal and spatial averages converge to the ensemble average? Lumley and Panofsky (1964) investigated this formulation of the question and were able to answer it in a simple, one-dimensional case. Anticipating a stationary random function of time that has an integral time scale, Lumley and Panofsky were able to derive mathematically a formula for the statistical error that should be a measure of

the difference between the time and the ensemble average. Lumley and Panofsky found that the ensemble average variance between the temporal average and the ensemble average is proportional to the ratio of the integral time scale and the averaging period. This implies that in order to make a meaningful interpretation of experimental measurements of a process, a single realization must be itself an ensemble, that is different sections of the record must be asymptotically regarded as independent experiments. In this case the statistical sampling error variance reduces inversely proportional to the numbers of degrees of freedom (given by the ratio of the averaging interval and the integral time scale). Based on this analysis Wyngaard (1983) demonstrated that a flight path over 1000 km might be needed to ensure statistical reliability of the averaging process of second-order moments for an integral scale of about 500 m. If the average was taken over a square area, then a 1000-km line average would be equivalent to an average over about a 25-km square. This is generally larger than the LES domain (here a 3.2-km square is used). Since the external forcing for the stratocumulus case considered here is assumed to be horizontally homogeneous it is reasonable to expect that the simulated turbulent flow is homogeneous in horizontal planes, i.e. the statistical averages should be invariant with respect to translation. However, since in the atmosphere integral scales are relatively large relative to the domain size, horizontal averages are expected not to be statistically reliable, while further averaging over time (thus increasing the number of realizations) should improve reliability.

To demonstrate this, ensemble runs of the stratocumulus case have been performed. The ensemble consists of 21 realizations of the process and uses the same numerical setup as described in Section 3, but differs in that different sets of spatially uncorrelated random perturbations uniformly distributed between -0.1 and 0.1 K are used to initialize the temperature field. Figure 1 shows instantaneous profiles (horizontal averages over the whole domain) of, (a) total (resolved plus subgrid-scale) vertical velocity variance, (b) total (resolved plus subgrid-scale) buoyancy flux, (c) total (resolved plus subgrid-scale) water flux, and (d) precipitation flux obtained from these ensemble runs at $t = 9000$ s. The ensemble average is marked using a thick black line. The profiles are widely scattered, indicating that the one-time area average is not sufficient to produce reliable statistics for second-order moments. The time average of the various profiles is then computed for a period of one hour centred at $t = 9000$ s where all time steps are taken into account. The results are displayed in Figure 2. It is evident that the statistical error is reduced after the time average. However, divergence of the individual realizations from the ensemble average is still evident. This suggests that a longer time averaging period or a larger domain may be required to encompass more large-scale eddies.

The noise reduction due to the utilization of a larger model domain is illustrated in Figure 3, which shows time averaged profiles of total buoyancy flux at $t = 2.5$ h for, (a) the standard domain of size $3.2 \times 3.2 \times 1.5$ km³ (left panel) and, for (b) the extended domain of size $28.8 \times 3.2 \times 1.5$ km³ (right panel). The thick full lines are used to denote the one-hour averages whereas the thin full lines are used

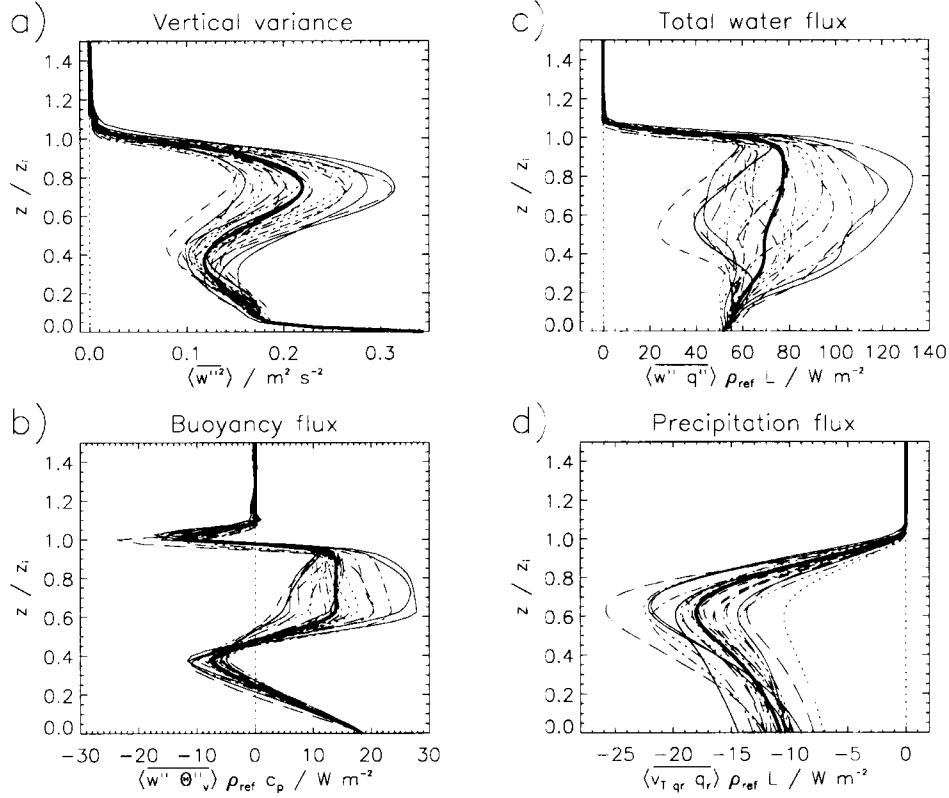


Figure 1. Vertical profiles of total vertical velocity variance (a), total buoyancy flux (b), total water flux (c), and precipitation flux (d) at $t = 9000$ s generated from 21 LES-model realizations of the stratocumulus case. The thick black line refers to the ensemble average.

to depict the non-overlapping five-minute averages (the scatter of these short-time averages is a measure of variability that would occur in ensemble experiments that utilize different initial conditions, and hence indicate the sampling error inherent in the area averaging), which are taken within the one-hour averaging interval. It is obvious that the standard deviation of the one-hour average reduces considerably when using the extended domain as a result of the increased number of large-scale eddies captured within the computational domain.

4.2. SENSITIVITY OF LES RESULTS WITH RESPECT TO THE REPRESENTATION OF SGS MIXING AND MICROPHYSICAL PROCESSES

The fundamental approach of LES is to explicitly resolve large turbulent eddies, which contain most turbulent kinetic energy and contribute most to transport. Although LES explicitly resolves the most important eddies, uncertainties still exist in these simulations. There is always uncertainty due to numerics and due to the treatment of small-scale turbulent motions through a subgrid-scale (SGS) model.

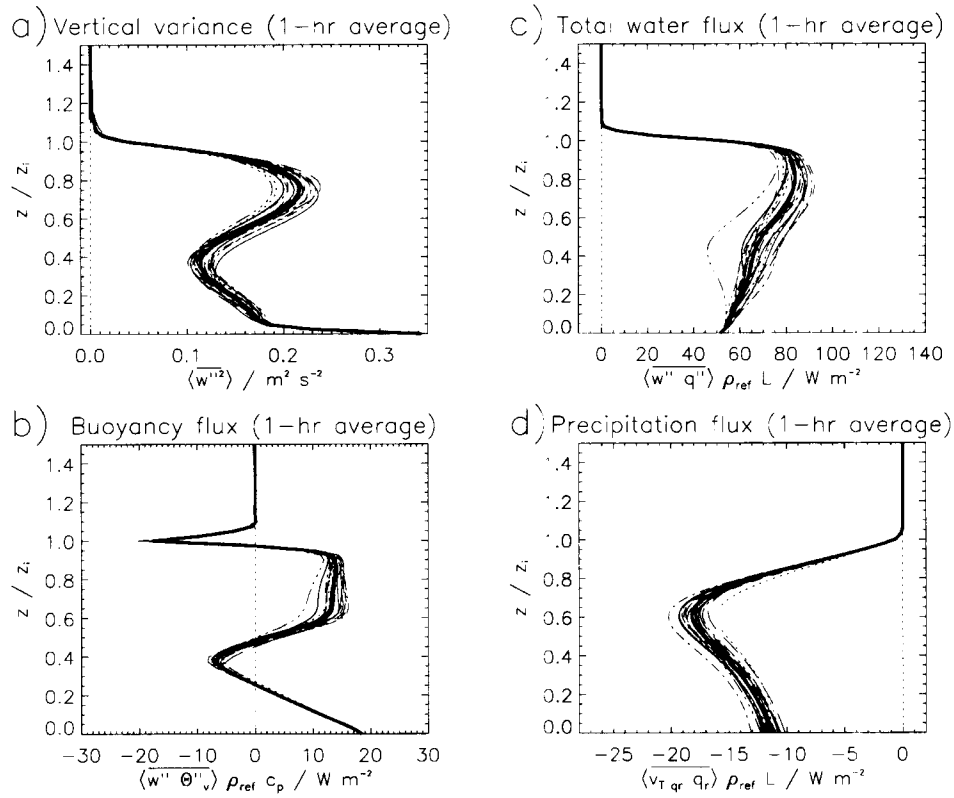


Figure 2. As in Figure 1 except profiles of time-averaged quantities from 7200 s to 10800 s.

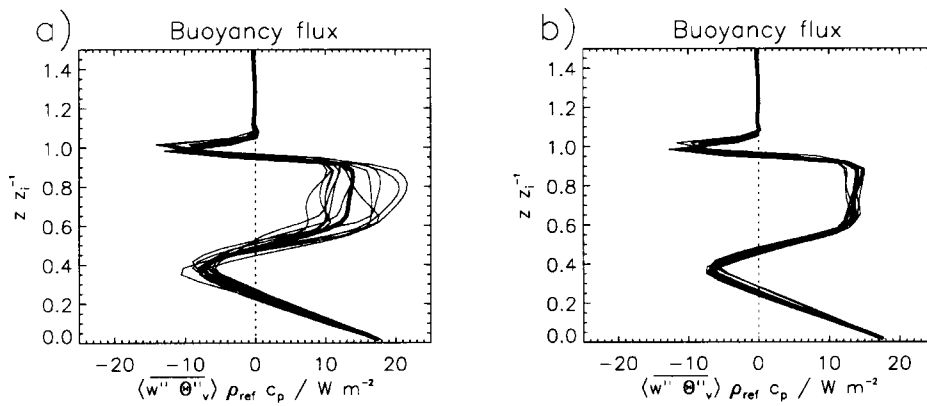


Figure 3. Time averaged vertical profiles of total buoyancy flux at $t = 2.5$ h for (a) the standard domain of size $3.2 \times 3.2 \times 1.5 \text{ km}^3$ (left panel) and for (b) the extended domain of size $28.8 \times 3.2 \times 1.5 \text{ km}^3$ (right panel). The thick full lines are used to denote the one-hour averages whereas the thin full lines are used to depict the non-overlapping five-minute averages which are taken within the one-hour averaging interval.

Moreover, in a cloud-topped boundary layer other uncertainties arise from the fact that the effects of condensation/evaporation and precipitation are parameterized processes in LESs.

To examine the sensitivity of our LES results arising from the inability to correctly represent physical processes we have performed, beside the reference run, three additional runs. The reference run is labelled REFERENCE and uses the SGS scheme of Deardorff and Lüpkes' microphysical scheme. The run KESSLER refers to the run that uses Deardorff's SGS scheme and Kessler's microphysical scheme. Likewise, the run SCHUMANN uses Schumann's SGS scheme and Lüpkes' microphysical scheme. Finally, the run NO RAIN refers to a nonprecipitating stratocumulus simulation that applies Deardorff's SGS scheme (for a brief description of the main characteristics of the schemes see Section 2). All runs utilize the same model initialization and forcing (see Section 3) and use the standard computational domain of size $3.2 \times 3.2 \times 1.5 \text{ km}^3$.

Figure 4 displays the time evolution of, (a) the inversion height, (b) the liquid water path (LWP), and (c) the precipitation rate for all runs. We see that all runs produce a boundary-layer top that rises from 705 m to about 775–805 m at the end of the simulation. The deepest boundary layer is found in the run NO RAIN. Note that the time variation of the boundary-layer top is directly proportional to the entrainment rate, as it is given by the difference between the entrainment velocity and the large-scale subsidence. All versions of the model produce a solid cloud cover and the LWP decreases in all runs during the course of integration. The final values for the LWP vary between 70 and 120 g m^{-2} , with NO RAIN having the largest and KESSLER having the smallest. Finally, the precipitation rate at the surface attains a final value varying between 0 and 0.2 mm d^{-1} . To summarize, the run NO RAIN produces the deepest boundary layer and the largest LWP. The effect of drizzle is to reduce the entrainment rate and, as a consequence of the direct removal of liquid water by droplet settling, to decrease the LWP. However, the results of the runs REFERENCE and KESSLER, which utilize different parameterization schemes to represent the precipitation process, differ noticeably but show only small differences in the modelled target variables. A different treatment of SGS processes in the LES model leads to insignificant changes in the properties of the modelled stratocumulus layer.

Figure 5 illustrates the vertical profiles of, (a) liquid water content, (b) total (resolved plus subgrid-scale) buoyancy flux, (c) total (resolved plus subgrid-scale) water flux, (d) precipitation flux, (e) total (resolved plus subgrid-scale) vertical velocity variance, and (f) total turbulent kinetic energy (resolved plus subgrid-scale) (TKE) for all runs. The profiles represent time averages over hours 2 to 3. The vertical axes have been scaled using the inversion height z_i . Overall, the runs that use a drizzle parameterization produce very similar results: the peak liquid water content varies between 0.45 and 0.52 g kg^{-1} , the maximum buoyancy flux occurs in the cloud layer and amounts to about 13 W m^{-2} , the total water flux is approximately linear between the surface and cloud top (maximum value about

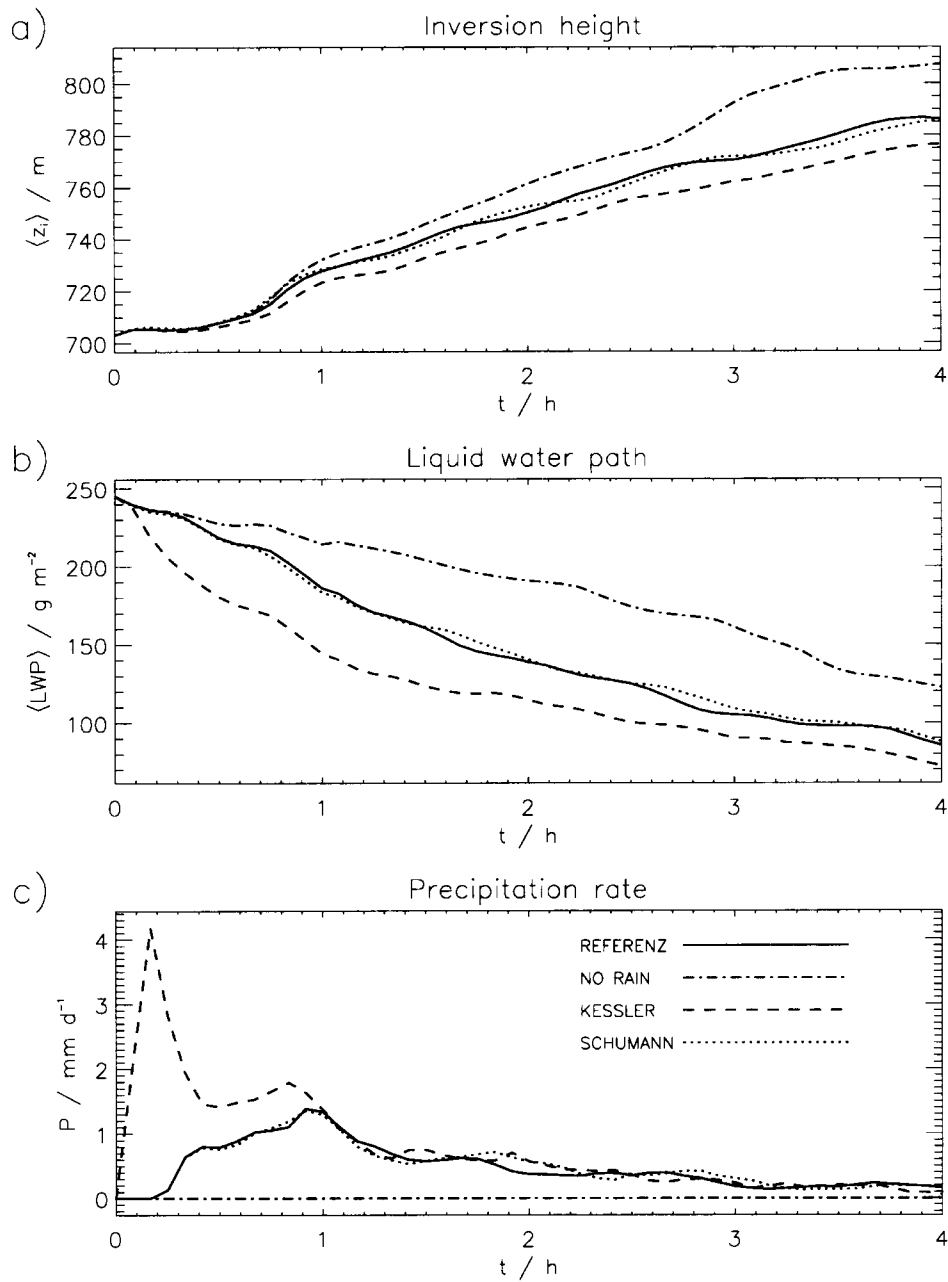


Figure 4. Time evolution of (a) the inversion height, (b) the liquid water path (LWP), and (c) the precipitation rate for four LES runs. Definition of line pattern is given in the legend of this figure. The simulation REFERENZ uses the SGS-scheme of Deardorff and Lüpkes' microphysical scheme. The simulation KESSLER refers to the run that uses Deardorff's SGS scheme and Kessler's microphysical scheme; the run SCHUMANN uses Schumann's SGS scheme and Lüpkes' microphysical scheme. Finally, the run NO RAIN refers to a nonprecipitating stratocumulus simulation which applies Deardorff's SGS scheme.

75 W m^{-2}), the maxima of the precipitation flux occur around $z/z_i = 0.6$ and vary between -11 and -18 W m^{-2} , the profiles of the total vertical velocity variance and the total turbulent kinetic energy exhibit two distinct maxima, one in the surface layer and a secondary maximum within the cloud layer. In the cloud layer the subgrid scales contribute less than 15% of the total vertical variance whereas they support a significant amount (about 90%) of vertical variance in the near-surface region. This implies that the model predictions for near-surface quantities are not as reliable as for those in the bulk of the boundary layer. However, our results are consistent with Monin–Obukhov similarity for unstable conditions and in excellent agreement with experimental data described by Wyngaard et al. (1971), who found that in the unstable surface layer the normalized variance ratio $\langle w^2 \rangle / u_*^2$ should vary between 2 and 4. In comparing results from the run NO RAIN with those that have the drizzle parameterization included, we note that the simulation of nonprecipitating stratocumulus produces more buoyant production of TKE resulting in enhanced energy and vertical velocity levels. Moreover, consistent with the variation of the LWP we found also larger values of the peak liquid water content in the NO RAIN run. Finally, the NO RAIN run also predicts the largest total water fluxes near cloud top. This is understandable because the cloud-top value is closely related to the entrainment rate prediction. According to a first-order jump model, $\overline{(wq)_{\text{inv}}} = -w_e \Delta \bar{q}$, where $\overline{(wq)_{\text{inv}}}$ denotes the total water entrainment flux right beneath the cloud top level, w_e is the entrainment rate, and $\Delta \bar{q}$ is the jump of the mean total water content across the cloud top. Therefore, a large entrainment rate would result in a larger total water entrainment flux and vice versa.

To see more clearly why the precipitating LES entrains less than the nonprecipitating LES we compute and analyse the budgets of resolvable-scale turbulent kinetic energy \bar{E} for the runs REFERENCE and KESSLER. The balance between the production, destruction and redistribution of \bar{E} as function of height in LES reads

$$\begin{aligned} \frac{\partial}{\partial t} \langle \bar{E} \rangle &= \frac{g}{\theta_{v00}} \langle \bar{w}'' \bar{\theta}_v'' \rangle - \langle \bar{u}'' \bar{w}'' \rangle \frac{d}{dz} \langle \bar{u} \rangle - \langle \bar{v}'' \bar{w}'' \rangle \frac{d}{dz} \langle \bar{v} \rangle \\ &\quad - \frac{d}{dz} \left(\langle \bar{w}'' \bar{E}'' \rangle + \frac{\langle \bar{w}'' \bar{\pi}'' \rangle}{\rho_{00}} \right) - \epsilon, \end{aligned} \quad (8)$$

where $\bar{E} = (\bar{u}''^2 + \bar{v}''^2 + \bar{w}''^2)/2$ and $\bar{\pi}''$ is the resolvable-scale pressure perturbation. A double-prime indicates the resolvable-scale fluctuation, an overbar denotes the Reynolds average and the brackets mean the horizontal average. In Equation (8) the term on the left hand side is storage (STD); first term on the right hand side is the buoyancy production (BP), the second shear production (SP), the third turbulent and pressure transport (TR), and the fourth, the parameterized dissipation (DISS). The dominant terms in these budgets (Figure 6) are the buoyant production and the dissipation terms. The buoyancy is the main generation term throughout most of the cloud layer, except near cloud top where the transport term is the dominant gain.

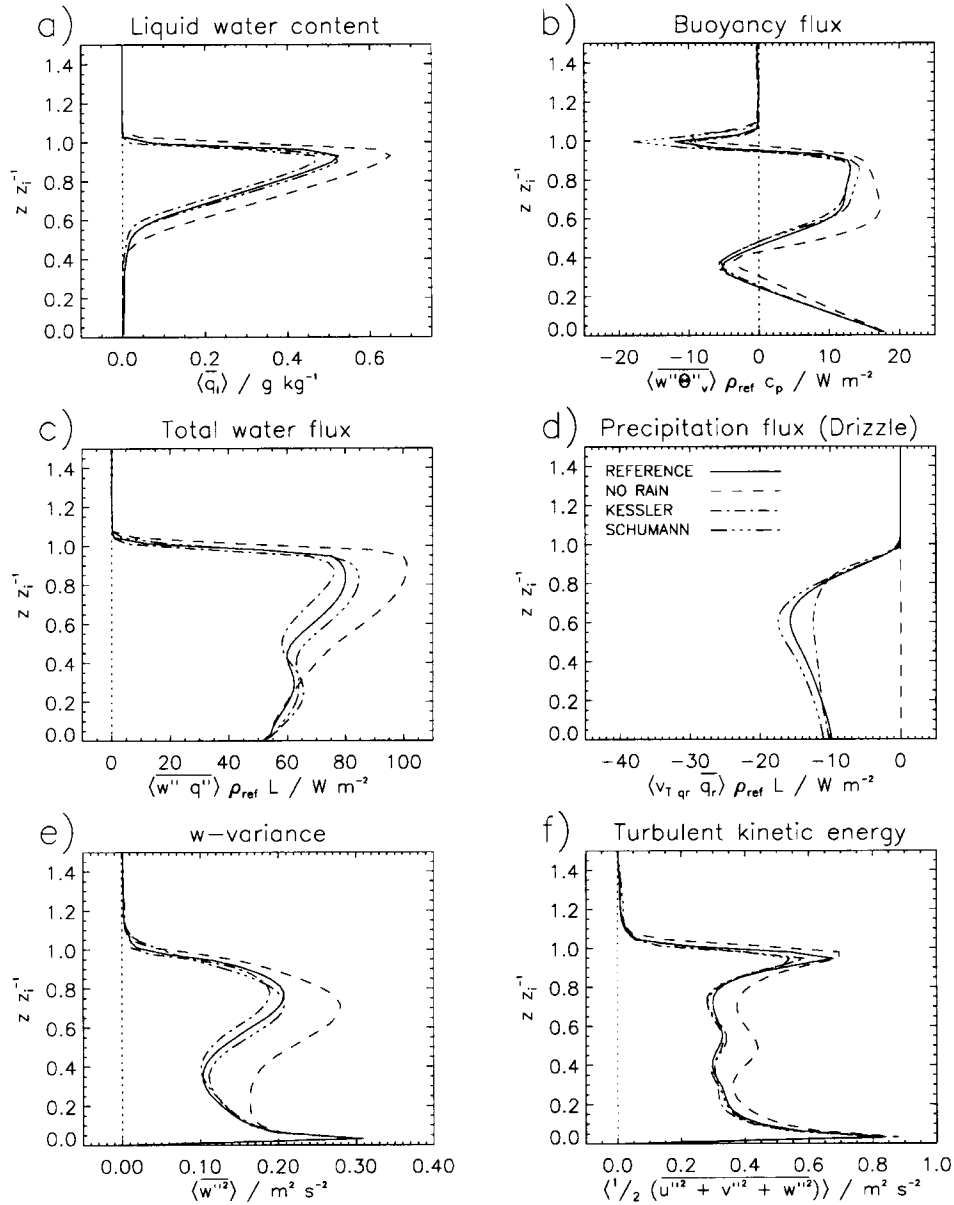


Figure 5. Vertical profiles of (a) liquid water content, (b) total buoyancy flux, (c) total water flux, (d) precipitation flux, (e) total vertical velocity variance, and (f) total turbulent kinetic energy (TKE) for four LES runs. The profiles represent time averages over hour 2 to 3. The vertical axes have been scaled using the inversion height z_i . Definition of line patterns is given in the legend of this figure.

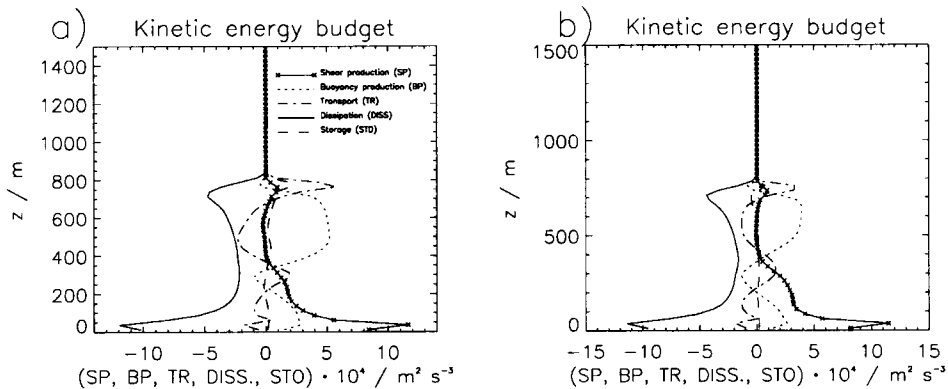


Figure 6. Profiles of various terms in the resolvable-scale turbulent kinetic energy budget for the simulations (a) NO RAIN (left panel) and (b) KESSLER (right panel). The profiles represent time averages over hour 2 to 3. Definition of line patterns is given in the legend of this figure.

The shear production term is small within the boundary layer but is significant near the surface. The most striking difference between the simulations is in the buoyancy production and transport terms. In the run REFERENCE the buoyancy production is larger and contributes over a deeper layer than in the run KESSLER; the greatest differences are between 300 and 500 m, in the vicinity of cloud base. This allows significant amounts of turbulent kinetic energy to be transported into the interfacial region between the cloud layer and the free atmosphere to do work against buoyancy forces necessary for mixing and entrainment to proceed at the observed rate.

To conclude, our study suggests that the primary dynamical effect of drizzle is to reduce the buoyant production of turbulent kinetic energy. Less production of turbulent kinetic energy results in a shallower boundary layer due to a reduction in entrainment rate. Drizzle also acts to limit the liquid water path (LWP) of stratocumulus. We found that the removal of water by drizzle lowered the maximum liquid water content near cloud top by about 20%. These key results have also been reported by Stevens et al. (1998). Admittedly, the prediction of the reduction of the maximum liquid water content near cloud top seems to be a rather trivial result since, because of the coalescence process, some cloud droplets are converted into rain drops, which are then subsequently removed by gravitational settling. Moreover, the predicted value of the liquid water depletion is rather uncertain as this number is strongly dependent on the precipitation scheme used; for example, the Kessler scheme utilizes a simple empirical relationship to parameterize the autoconversion process. This formulation makes use of an autoconversion threshold value of the cloud water content that must be exceeded in order to induce rain. Indeed, Delobbe and Gallée (1998) demonstrated that the value of the autoconversion threshold has a large impact on the simulated cloud especially on its liquid water path. Another potential effect of drizzle is in its ability to promote

drying of the cloud layer and moistening of the subcloud layer. However, this decoupling procedure, by which the layer between the heating in the cloud layer and the cooling in the subcloud layer is stabilized, was not encountered in the nocturnal stratocumulus cases we have presented here because the simulated precipitation rates were too small to significantly alter the vertical distribution of latent heating. Finally, we found that the results of LESs turned out to be insensitive to the actual details of the subgrid model and to assumptions about the particular elements of the microphysical precipitation model.

4.3. SENSITIVITY OF LES RESULTS WITH RESPECT TO ENVIRONMENTAL CONDITIONS

A numerical model designed to simulate variables of interest in a given system can be tested by comparing model predictions with observations. Since both observations and predictions may be uncertain, meaningful model verification requires not only the average values but also some measure of the uncertainty of target variables.

In this section we address the parametric uncertainty of our LES results that arises because of the incomplete knowledge of model input parameters. In principle, parametric uncertainty can be reduced by refining measurements of input parameters. The importance of these parameters to model outputs can be ranked by using a sensitivity analysis. In a sensitivity analysis we are interested in how the model outputs respond to small changes in a given uncertain parameter with all of the other parameters fixed. In this way the sensitivity analysis reveals the local gradient of the model response with respect to a given parameter. Here, we examine the sensitivity of our LES results with respect to the assumed values of various external, environmental conditions. These conditions include all those environmental parameters that are needed to specify all of the mean initial and boundary conditions required to run a model simulation. Our study investigates the sensitivity of the model output with respect to the following parameters: (a) the inversion strength in total water content $(\Delta \bar{q})_{\text{inv}}$, (b) the inversion strength in liquid water potential temperature $(\Delta \bar{\theta}_l)_{\text{inv}}$, (c) the large-scale subsidence w_{LS} , (d) the sea surface flux of heat $(\overline{w\theta})_{\text{SFC}}$, (e) the sea surface flux of moisture $(\overline{wq})_{\text{SFC}}$, and (f) the net longwave radiative cooling $F_{\text{NET}}^{\text{CT}}$. Uncertainties in these external input parameters may arise from instrumental measurement errors, sampling errors, and the nonstationarity and spatial inhomogeneities of the fields under consideration during the measurements.

In general the total modelled uncertainty depends on these parameters in a complicated and often counterintuitive way. Nevertheless, it is important that quantitative estimates of these uncertainties be derived, as a means of assigning error bars to the LES-derived data products. In the following we present a methodology for objective determination of the uncertainty in LES-derived quantities.

The methodology is based on standard error-propagation procedures and yields expressions for probable error as a function of the relevant parameters.

For any LES-derived function Ψ (i.e., q_l , $\langle w\theta_v \rangle$, $\langle wq_l \rangle$, $\langle w^2 \rangle$) that depends on several measured environmental parameters u, v, \dots (i.e., $(\Delta\bar{q})_{\text{inv}}$, $(\Delta\bar{\theta}_l)_{\text{inv}}$, w_{LS} , $(\overline{w\theta})_{\text{SFC}}$, $(\overline{wq})_{\text{SFC}}$, $F_{\text{NET}}^{\text{CT}}$) the uncertainty σ_Ψ (standard deviation) in Ψ can be approximated as:

$$\sigma_\Psi^2 = \left(\frac{\partial \Psi}{\partial u} \right)^2 \sigma_u^2 + \left(\frac{\partial \Psi}{\partial v} \right)^2 \sigma_v^2 + 2C_{uv} \left(\frac{\partial \Psi}{\partial u} \right) \left(\frac{\partial \Psi}{\partial v} \right) + \dots, \quad (9)$$

where σ_u is the uncertainty in the measured parameter u and C_{uv} is the covariance between the measured parameters u and v . Assuming uncorrelated measurement errors we find

$$\sigma_\Psi = \sqrt{\sum_i \left(\frac{\partial \Psi}{\partial x_i} \right)^2 \sigma_{x_i}^2}, \quad (10)$$

where x_i ($i = 1, 6$) denote the external, environmental parameters, that is, $x_1 = (\Delta\bar{q})_{\text{inv}}$, $x_2 = (\Delta\bar{\theta}_l)_{\text{inv}}$, $x_3 = w_{\text{LS}}$, $x_4 = (\overline{w\theta})_{\text{SFC}}$, $x_5 = (\overline{wq})_{\text{SFC}}$, and $x_6 = F_{\text{NET}}^{\text{CT}}$. Thus, the total uncertainty (standard deviation) of a LES-derived quantity Ψ contains contributions from uncertainties due to thermodynamic measurements of cloud-top jumps in liquid water potential temperature and total water content, errors in the estimation of the large-scale subsidence and surface fluxes, and errors in the assumed value of the net radiative cooling. To evaluate the above equation we must first evaluate the partial derivative of Ψ with respect to the parameters x_i . This has been done by performing 12 LES runs in which one of the parameters x_i has been varied (positively and negatively around its central value) while the others have been kept fixed to their original values. The partial derivative is then calculated using a second-order accurate finite difference approximation. All runs use the extended computational domain of size $28.8 \times 3.2 \times 1.5 \text{ km}^3$.

In particular, the purpose of the parametric sensitivity analysis in this case is to find the uncertainty of LES-generated vertical profiles of various quantities (that is, liquid water content, buoyancy flux, total water flux, precipitation flux, total vertical variance, and total turbulent kinetic energy) given the uncertainties (standard deviations) in the uncertain input parameters. With respect to the jumps in liquid water potential temperature and total water content, we assume that these values are accurate to within $\pm 1 \text{ K}$ and $\pm 0.5 \text{ g kg}^{-1}$, respectively. With respect to the large-scale subsidence, the surface fluxes of heat and moisture, and the net longwave radiative cooling we anticipate that these quantities can be estimated from the measurements with an accuracy of 25%. Central values and uncertainty factors (standard deviations) of the external, environmental input parameters are listed in Table I.

TABLE I

Central values and uncertainty factors (standard deviations) of the external, environmental input parameters.

Parameter	Central value	Standard deviation
$(\Delta\bar{\theta})_{\text{inv}}$ (K)	5.5	1
$(\Delta\bar{q})_{\text{inv}}$ (g kg ⁻¹)	-1.6	0.5
w_{LS} (m s ⁻¹)	-0.0225	0.00565
$(\overline{w\theta})_{\text{SFC}}$ (W m ⁻²)	14.9	3.725
$(\overline{wq})_{\text{SFC}}$ (W m ⁻²)	51.5	12.875
$F_{\text{NET}}^{\text{CT}}$ (W m ⁻²)	74	18.5

Figure 7 presents the vertical profiles of, (a) liquid water content, (b) total (resolved plus subgrid-scale) buoyancy flux, (c) total (resolved plus subgrid-scale) water flux, (d) precipitation flux, (e) total (resolved plus subgrid-scale) vertical velocity variance, and (f) total (resolved plus subgrid-scale) turbulent kinetic energy (TKE) for the reference run, which utilizes the central values for the input parameters. The profiles represent time averages over hour 2 to 3. The vertical axes have been scaled using the inversion height z_i . Data are marked with diamonds and refer to aircraft measurements during the flight ASTEX RF06 (after de Roode and Duynkerke, 1997). In addition, 90% confidence limits (that is, $\pm 1.6\sigma$ intervals) have been plotted at selected height levels for the various quantities. Apart from the confidence limits, the sensitivity analysis also provides a framework for ranking the uncertain parameters according to their contribution to the total model variance. Table II gives means and standard deviations of various quantities (that is, $\langle q_l \rangle$, $\langle w\theta_v \rangle$, $\langle wq_l \rangle$, $\langle w_{\text{sed}}q_r \rangle$, $\langle w^2 \rangle$, $0.5(\langle u^2 \rangle + \langle v^2 \rangle + \langle w^2 \rangle)$) at selected heights as well as of the entrainment rate w_e , the liquid water path and the convective scaling velocity w^* . In addition, normalized variance contributions (in percent) from variations of external input parameters x_i (that is, $(\Delta\bar{q})_{\text{inv}}$, $(\Delta\bar{\theta})_{\text{inv}}$, w_{LS} , $(\overline{w\theta})_{\text{SFC}}$, $(\overline{wq})_{\text{SFC}}$, $F_{\text{NET}}^{\text{CT}}$) to the total variance σ_Ψ^2 of a modelled quantity Ψ are also listed.

Overall, with the exception of the precipitation flux, the model predictions of thermodynamic, dynamic and microphysical properties are generally in reasonable agreement with the measurements during flight ASTEX RF06 obtained in a stratocumulus-topped boundary layer. The differences between the model and measurements are (with the exception of the precipitation flux) within the modelling uncertainties.

In particular, the measured as well as the computed liquid water content increase with height in the cloud and reach a maximum at $z/z_i = 0.9$. This shows that entrainment leads to a decrease in the liquid water content just below cloud top. A peak value in the liquid water content of 0.44 g kg⁻¹ was reported by de Roode

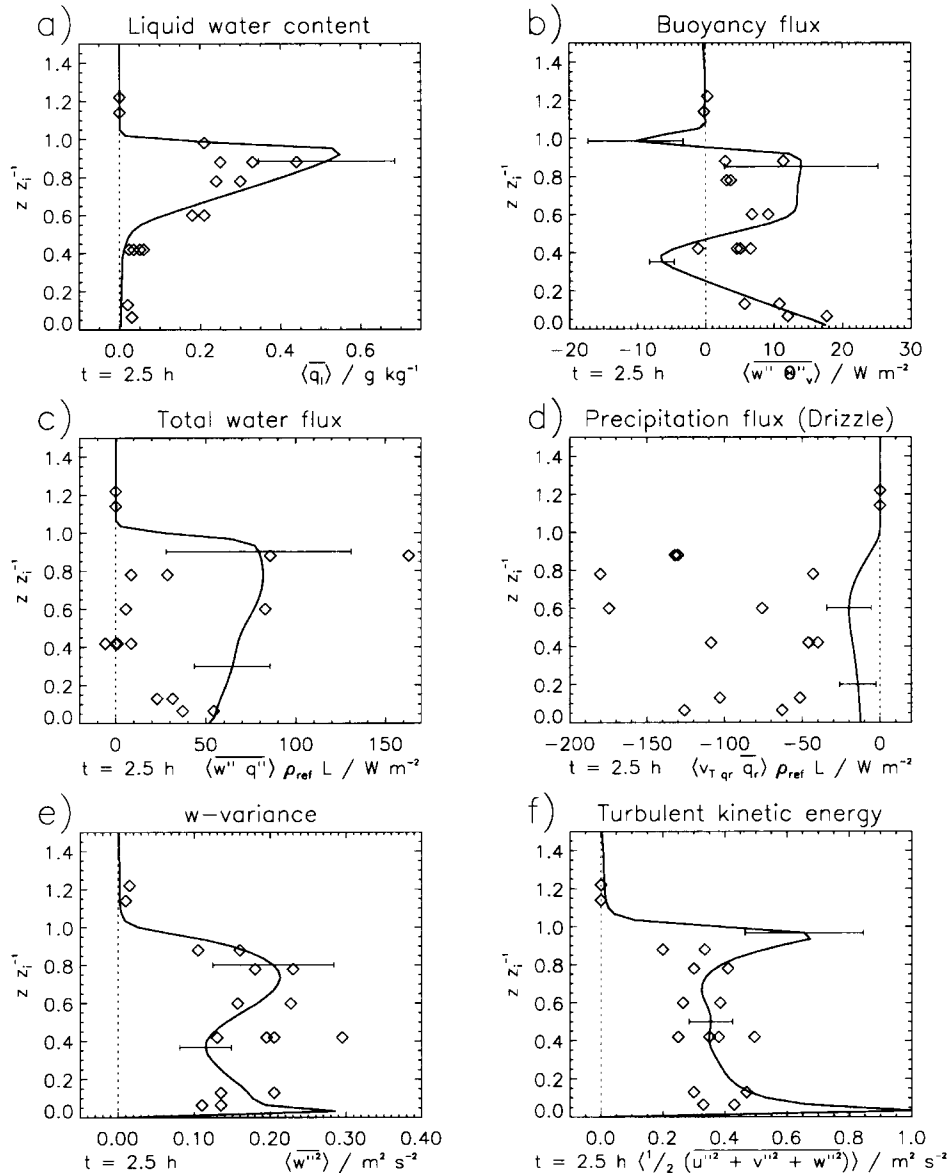


Figure 7. Vertical profiles of (a) liquid water content, (b) total buoyancy flux, (c) total water flux, (d) precipitation flux, (e) total vertical velocity variance, and (f) total turbulent kinetic energy (TKE) for the reference run which utilizes the central values for the input parameters. The profiles represent time averages over hour 2 to 3. The vertical axes have been scaled using the inversion height z_i . Data are marked with diamonds and refer to aircraft measurements during the flight ASTEX RF06 (after de Roode and Duynkerke (1997)). In addition, 90% confidence limits (that is, $\pm 1.6\sigma$ intervals) have been plotted at selected height levels for the various quantities.

TABLE II

Means and standard deviations of various quantities (that is, $\langle q_l \rangle$, $\langle w\theta_v \rangle$, $\langle wq_t \rangle$, $\langle w_{\text{sed}qr} \rangle$, $\langle w^2 \rangle$, $0.5x(\langle u^2 \rangle + \langle v^2 \rangle + \langle w^2 \rangle)$) at selected normalized heights as well as of the entrainment rate w_e , the liquid water path (LWP), and the convective scaling velocity w^* . In addition, normalized variance contributions (in percent) from variations of external input parameters x_i (that is, $x_1 = (\Delta\bar{q})_{\text{inv}}$, $x_2 = (\Delta\bar{\theta})_{\text{inv}}$, $x_3 = w_{\text{LS}}$, $x_4 = (\overline{w\theta})_{\text{SFC}}$, $x_5 = (\overline{wq})_{\text{SFC}}$, $x_6 = F_{\text{NET}}^{\text{CT}}$) to the total variance σ_{Ψ}^2 of a modelled quantity Ψ are also listed.

Quantity	Mean	Standard deviation	Normalized variance contributions (in percent) by various parameters					
			x_1	x_2	x_3	x_4	x_5	x_6
$\langle q_l \rangle$ ($z/z_i = 0.9$)/(g kg ⁻¹)	0.52	0.11	68.0	8.5	15.0	0	0	8.5
$\langle w\theta_v \rangle$ ($z/z_i = 0.35$)/(W m ⁻²)	-6.0	1.2	50.0	0	0	0	0	50.0
$\langle w\theta_v \rangle$ ($z/z_i = 0.85$)/(W m ⁻²)	14.0	7.1	66.9	6.9	0	0.7	0.7	24.8
$\langle w\theta_v \rangle$ ($z/z_i = 1.0$)/(W m ⁻²)	-10.5	4.4	71.2	10.9	0	0	0	17.9
$\langle wq_t \rangle$ ($z/z_i = 0.30$)/(W m ⁻²)	64.0	13.1	22.5	0	0	0	62.5	15.5
$\langle wq_t \rangle$ ($z/z_i = 0.90$)/(W m ⁻²)	79.0	31.0	57.2	25.5	0	0	5.5	11.8
$\langle w_{\text{sed}qr} \rangle$ ($z/z_i = 0.20$)/(W m ⁻²)	-13.0	7.3	57.9	0	29.2	0	0	12.9
$\langle w_{\text{sed}qr} \rangle$ ($z/z_i = 0.60$)/(W m ⁻²)	-20.0	8.9	49.4	0	32.8	0	0	17.8
$\langle w^2 \rangle$ ($z/z_i = 0.35$)/(m ² s ⁻²)	0.12	0.021	0	0	0	50.0	0	50.0
$\langle w^2 \rangle$ ($z/z_i = 0.80$)/(m ² s ⁻²)	0.21	0.05	15.8	0	0	0	4.0	80.2
TKE ($z/z_i = 0.50$)/(m ² s ⁻²)	0.35	0.05	20.0	0	0	0	0	80.0
TKE ($z/z_i = 0.95$)/(m ² s ⁻²)	0.65	0.12	55.5	0	0	0	11.0	33.5
w_e /(cm s ⁻¹)	1.7	0.50	12.2	62.5	0	3.8	1.1	20.4
LWP/(g m ⁻²)	116.0	39	69.0	0.8	21.0	0	0.1	8.2
w^* /(cm s ⁻¹)	0.71	0.055	20.2	0	0	20.2	16.4	43.0

and Duynkerke (1997), whereas the model predicts an interval (90% confidence interval) of possible peak values between 0.38–0.72 g kg⁻¹. The inversion jump in total water ($\Delta\bar{q}$)_{inv} makes the largest contribution to the model variance, where larger jumps in ($\Delta\bar{q}$)_{inv} produce smaller peak values in liquid water content and vice versa (see Table II).

Figure 7b presents the vertical distribution of the observed and modelled total (resolved plus subgrid-scale) buoyancy flux. The maximum buoyancy flux is found in the upper part of the cloud layer in both the observations and in the model. This implies that cloud-top cooling due to the evaporation of cloud droplets and radiation are the dominant buoyancy production mechanisms. The model predicts an uncertainty interval for the buoyancy flux of 3–25 W m⁻² at this height where the parameters ($\Delta\bar{q}$)_{inv} and $F_{\text{NET}}^{\text{CT}}$ make the largest contribution to the model variance (see Table II). The modelled buoyancy flux is negative near the inversion and is due to the entrainment that takes potentially warmer and drier air from above

the inversion into the cloud (since entrainment occurs only over a small height interval it has not been measured). At lower levels in the cloud, the observed and the modelled buoyancy flux decrease downward to small or even negative values near cloud base.

Figure 7c shows the total (resolved plus subgrid-scale) water flux, which varied greatly in the observations. The modelled total water flux is approximately linear between the surface and the upper part of the cloud layer. The maximum at $z/z_i = 0.9$ is due to the entrainment of dry air from above the cloud. The predicted uncertainty range is rather large ($\pm 50 \text{ W m}^{-2}$ at $z/z_i = 0.9$) and is mainly caused by the uncertainty in the parameter $(\Delta\bar{q})_{\text{inv}}$ (see Table II). In view of these large uncertainties the modelled total water flux appears not inconsistent with the observations.

The most apparent discrepancy between results obtained from the model and observations can be detected in the precipitation flux (Figure 7d). The measured precipitation fluxes indicate that in the cloud layer the drizzle flux is of the same order of magnitude as the total water flux. Moreover, from the lowest legs during Flight RF06, it is observed that drizzle effectively reached the surface (with surface precipitation flux around -100 W m^{-2}), thereby removing water from the boundary layer. In contrast, the calculated drizzle fluxes are about one order of magnitude smaller than the observed fluxes. It is well known that the precipitation rate can vary much with space and time, with local rain rates 4 to 5 times larger than the replacement moisture flux (Austin et al., 1995). For that reason the correct representation of the precipitation process within a numerical model appears hardly manageable and remains a challenging task. At the moment we cannot find any plausible explanation for the apparent inability of the model to match correctly the observed drizzle rates during heavy rainfall from stratocumulus clouds. In light of the fact that precipitation in stratocumulus clouds affects, as pointed out in Section 4.2, the planetary boundary-layer structure and cloud fraction in a climatologically significant way, we recommend that the principle dynamical interactions in precipitating stratocumulus layers should be investigated more intensively in the future.

The total (resolved plus subgrid-scale) vertical variance and total turbulent kinetic energy (TKE) profiles are displayed in Figures 7e and 7f, respectively. The modelled profiles of the total vertical velocity variance and the total TKE exhibit two distinct maxima, one near the surface layer and a secondary maximum within the cloud layer indicating that the convection driven from the surface due to a positive surface buoyancy flux is as important as the convection driven from the cloud top. The modelled magnitude of the vertical velocity variance and the TKE is in a good agreement with the observations. The parameters $(\Delta\bar{q})_{\text{inv}}$, $F_{\text{NET}}^{\text{CT}}$ and $(\overline{w\theta})_{\text{SFC}}$ make the largest contributions to the modelled uncertainties (see Table II).

Finally, we note that values of the entrainment rate w_e and the convective velocity scale w^* reported by de Roode and Duynkerke (1997) compare well with

those calculated by the model, as they are within the predicted confidence limits (see Table II).

5. Summary and Conclusions

Results of three-dimensional numerical calculations of the stratocumulus-topped boundary layer have been presented, using the large-eddy-simulation (LES) technique. The LES model has been tested against the observed structure of a marine stratocumulus layer obtained during flight RF06 of the first Lagrangian experiment of the Atlantic Stratocumulus Transition Experiment (ASTEX). In this paper we have studied three related aspects of LES in the stratocumulus-topped boundary layer by focusing on some aspects of parametric and structural uncertainty. In particular, we have addressed the following items:

1. Ensemble runs have been performed to give 21 realizations of the simulation. Examination of profiles of the predicted mean fluxes at a particular instant of time (150 min after the initial time) showed considerable spread among the ensemble members. The spread was reduced, but was still not negligible, when the results were displayed as 1-hr averages. An additional run was done for a domain nine times larger in the cross-wind direction. The spreading was reduced still further for the 1-hr averages over the larger domain. These results indicate the need for care in interpreting results from a single model run, and demonstrate that averaging should be done over sufficiently large temporal and spatial domains.
2. A number of runs were done to test the sensitivity of the results to Deardorff's and Schumann's subgrid-scale scheme, and to Kessler's and Lüpkes's, cloud microphysics schemes, as well as to a 'no-rain' scheme. The Deardorff/no rain run produced the deepest boundary layer and the largest liquid-water path. The impacts of the different subgrid schemes were small, but the primary effects of drizzle in the Kessler or Lüpkes runs were to reduce the buoyant production of turbulent kinetic energy, resulting in shallower boundary layers due to reduced entrainment rates. The removal of water by drizzle lowered the maximum liquid water content near the cloud top by 20%.
3. We have examined the sensitivity of our LES results with respect to the assumed values of various external, environmental conditions. These conditions include all those environmental parameters that are needed to specify all of the mean initial and boundary conditions required to initiate a model simulation. Simplified linear relationships between the variances of simulated quantities and the variances of measured environmental parameters were used to assess the sensitivity of the model to initial data uncertainties. The coefficients in these relationships, which depend on the gradients of simulated quantities with respect to the observed parameters, were estimated from a limited number of sensitivity runs. The exercise enabled error bars to be estimated

for the simulations. Overall, with the exception of the precipitation flux, the model predictions of thermodynamic, dynamic and microphysical properties are generally in reasonable agreement with the measurement made during the flight ASTEX RF06 obtained in a stratocumulus-topped boundary layer. The differences between the model and measurements are within the modelling uncertainties, but the calculated precipitation rate differs significantly from that observed. Apart from the confidence limits, the sensitivity analysis also provided a framework for ranking the uncertain parameters according to their contribution to the total model variance. We found that the largest contribution to the variance of the LES-derived data products is due to the uncertainties in the cloud-top jump of total water mixing ratio and the net radiative forcing. However, the calculated precipitation rate was found to differ significantly from that derived in the observations. Therefore, we conclude that the representation of the precipitation process within a numerical model of stratocumulus is difficult, and improving the results will prove to be a challenging task.

Finally, our LES calculations underline the importance of properly representing the coupling between boundary-layer clouds, precipitation, radiation and turbulence in cloud and boundary-layer parameterizations in a general circulation model (GCM). This is because the principle effect of precipitation is to affect the turbulent structure of the boundary layer in a climatologically significant way. Thus, only if the principle couplings between the various processes are captured in a GCM can such models be used in order to better understand the climatological importance of precipitation from boundary-layer clouds on the earth's climate.

Acknowledgements

The authors wish to thank Drs. H. Grassl and H. Hinzpeter for their useful comments and close interest in this study. We are very grateful to Dr. P. Duynkerke and S. de Roode of the Institute for Marine and Atmospheric Research Utrecht (IMAU) who kindly provided the aircraft measurements made during flight RF06 of the Atlantic Stratocumulus Transition Experiment (ASTEX). This work has received financial support by the CEC contract ENV4CT95-0107 EUCREM (European Cloud Resolving Modelling Program).

References

- Albrecht, B. A., Bretherton, C. S., Johnson, D., Schubert, W. H., and Frisch, A. S.: 1995, 'The Atlantic Stratocumulus Transition Experiment – ASTEX', *Bull. Amer. Meteorol. Soc.* **76**, 889–904.
- Austin, P., Wang, Y. , Pincus, R., and Kujala, V.: 1995, 'Precipitation in Stratocumulus Clouds: Observational and Modeling Results', *J. Atmos. Sci.* **52**, 232–490.

- Bougeault, P.: 1985, 'The Diurnal Cycle of the Marine Stratocumulus Layer: A Higher-Order Model Study', *J. Atmos. Sci.* **42**, 2826–2843.
- Bougeault, P. and André, J. C.: 1986, 'On the Stability of the Third Order Turbulence Closure for the Modelling of the Stratocumulus-Topped Boundary Layer', *J. Atmos. Sci.* **43**, 1574–1581.
- Chen, C. and Cotton, W. R.: 1987, 'The Physics of the Marine Stratocumulus-Capped Mixed Layer', *J. Atmos. Sci.* **44**, 2951–2977.
- Chlond, A.: 1992, 'Three-Dimensional Simulation of Cloud Street Development during a Cold Air Outbreak', *Boundary-Layer Meteorol.* **58**, 161–200.
- Chlond, A.: 1994, 'Locally Modified Version of Bott's Advection Scheme', *Mon. Wea. Rev.* **122**, 111–125.
- Deardorff, I. W.: 1976, 'On the Entrainment Rate of a Stratocumulus-Topped Mixed Layer', *Quart. J. Roy. Meteorol. Soc.* **102**, 563–582.
- Deardorff, J. W.: 1980, 'Stratocumulus-Capped Mixed Layers Derived from a Three-Dimensional Model', *Boundary-Layer Meteorol.* **18**, 495–527.
- Delobbe, L. and Gallée, H.: 1998, 'Simulation of Marine Stratocumulus: Effect of Precipitation Parameterization and Sensitivity to Droplet Number Concentration', *Boundary-Layer Meteorol.* **89**, 75–107.
- de Roode, S. R. and Duynkerke, P. G.: 1997, 'Observed Lagrangian Transition of Stratocumulus into a Cumulus during ASTEX: Mean State and Turbulence Structure', *J. Atmos. Sci.* **54**, 2157–2173.
- Duynkerke, P. G.: 1989, 'The Diurnal Variation of a Marine Stratocumulus Layer: A Model Sensitivity Study', *Mon. Wea. Rev.* **117**, 1710–1725.
- Duynkerke, P. G., Jonker, P. J., Chlond, A., van Zanten, M. C., Cuxart, J., Clark, P., Sanchez, F., Martin G., Lenderink, G., and Teixeira, J.: 1999, 'Intercomparison of Three- and One-Dimensional Model Simulations and Aircraft Observations of Stratocumulus', *Boundary-Layer Meteorol.* **92**, 453–487.
- Fravolo, C., Fouquart, Y., and Rosset, R.: 1981, 'The Sensitivity of a Model of Low Stratiform Clouds to Radiation', *J. Atmos. Sci.* **38**, 1049–1062.
- Hanson, H. P.: 1984, 'On Mixed-Layer Modeling of the Stratocumulus-Topped Marine Boundary Layer', *J. Atmos. Sci.* **41**, 1226–1234.
- Harrison, E. F., Minnis, P., Barkstrom, B. R., Ramanathan, V., Cess, R. D., and Gibson, C. G.: 1990, 'Seasonal Variation of Cloud Radiative Forcing Derived from the Earth Radiation Budget Experiment', *J. Geophys. Res.* **95**, 18687–18703.
- Kessler, E.: 1969, 'On the Distribution and Continuity of Water Substances in Atmospheric Circulation', *Meteorological Monographs*, No. 32, American Meteorological Society, 84 pp.
- Klein, S. A. and Hartmann, D. L.: 1993, 'The Seasonal Cycle of Stratiform Clouds', *J. Climate* **6**, 1587–1606.
- Kogan, Y. L., Khairoutdinov, M. P., Lilly, D. K., Kogan, Z. N., and Liu, Q.: 1995, 'Modeling Stratocumulus Cloud Layers in a Large-Eddy Simulation Model with Explicit Microphysics', *J. Atmos. Sci.* **52**, 2923–2940.
- Lilly, D. K.: 1968, 'Models of Cloud-Topped Mixed Layers under a Strong Inversion', *Quart. J. Roy. Meteorol. Soc.* **94**, 292–309.
- Lumley, J. L. and Panofsky, H. A.: 1964, *The Structure of Atmospheric Turbulence*, Interscience Publishers, New York, 239 pp.
- Lüpkes, C.: 1991, *Untersuchungen zur Parametrisierung von Koagulationsprozessen niederschlagsbildender Tropfen*, Verlag Dr. Kovac, Hamburg, 156 pp.
- Moeng, C.-H.: 1986, 'Large-Eddy Simulation of a Stratus-Topped Boundary Layer. Part I: Structure and Budgets', *J. Atmos. Sci.* **43**, 2886–2900.
- Moeng, C.-H. and Arakawa, A.: 1980, 'A Numerical Study of a Marine Subtropical Stratus Cloud Layer and its Stability', *J. Atmos. Sci.* **37**, 2661–2676.
- Moeng, C.-H. and Randall, D. A.: 1984, 'Problems in Simulating the Stratocumulus-Topped Boundary Layer with a Third-Order Closure Model', *J. Atmos. Sci.* **41**, 1588–1600.

- Moeng, C.-H., Lenschow, D. H., and Randall, D. A.: 1995, 'Numerical Investigations of the Roles of Radiative and Evaporative Feedbacks in Stratocumulus Entrainment and Breakup', *J. Atmos. Sci.* **52**, 2869–2883.
- Moeng, C.-H., Shen, S., and Randall, D. A.: 1992, 'Physical Processes within the Nocturnal Stratus-Topped Boundary Layer', *J. Atmos. Sci.* **49**, 2384–2401.
- Monin, A. S. and Yaglom, A. M.: 1971, *Statistical Fluid Mechanics: Mechanics of Turbulence*, Vol. 1, The MIT Press, Cambridge, MA, 769 pp.
- Müller, C. and Chlond, A.: 1996, 'Three-Dimensional Numerical Study of Cell Broadening during Cold-Air Outbreaks', *Boundary-Layer Meteorol.* **81**, 289–323.
- Oliver, D. A., Lewellen, W. S., and Williamson, C. C.: 1978, 'The Interaction between Turbulent and Radiative Transport in the Development of Fog and Low-Level Stratus', *J. Atmos. Sci.* **35**, 310–316.
- Piacsek, S. A. and Williams, C. P.: 1970, 'Conservation Properties of Convection Difference Schemes', *J. Comput. Phys.* **6**, 392–405.
- Ramanathan, V., Cess, R. D., Harrison, E. F., Minnis, P., Barkstrom, B. R., Ahmad, E., and Hartmann, D.: 1989, 'Cloud-Radiative Forcing and Climate: Results from the Earth Radiation Budget Experiment', *Science* **243**, 57–63.
- Randall, D. A.: 1984, 'Buoyant Production and Consumption of Turbulent Kinetic Energy in Cloud-Topped Mixed Layers', *J. Atmos. Sci.* **41**, 402–413.
- Rogers, D. P. and Koracin, D.: 1992, 'Radiative Transfer and Turbulence in the Cloud Topped Marine Atmospheric Boundary Layer', *J. Atmos. Sci.* **49**, 1473–1486.
- Schaller, E. and Kraus, H.: 1981a, 'The Role of Radiation in an Inversion Capped Planetary Boundary Layer. Part I: The Need for a Detailed Consideration of Radiative Processes', *Boundary-Layer Meteorol.* **20**, 485–495.
- Schaller, E. and Kraus, H.: 1981b, 'The Role of Radiation in an Inversion Capped Planetary Boundary Layer. Part II: The Internally Interactive Radiative-Convective Model', *Boundary-Layer Meteorol.* **20**, 497–518.
- Schubert, W. H.: 1976, 'Experiments with Lilly's Cloud-Topped Mixed Layer Model', *J. Atmos. Sci.* **33**, 436–446.
- Schubert, W. H., Wakefield, J. S., Steiner, E. J., and Cox, S. K.: 1979a, 'Marine Stratocumulus Convection. Part I: Governing Equations and Horizontally Homogeneous Solutions', *J. Atmos. Sci.* **36**, 1286–1307.
- Schubert, W. H., Wakefield, J. S., Steiner, E. J., and Cox, S. K.: 1979b, 'Marine Stratocumulus Convection. Part II: Horizontally Inhomogeneous Solutions', *J. Atmos. Sci.* **36**, 1308–1324.
- Schumann, U.: 1991, 'Subgrid Length-Scales for Large-Eddy Simulation of Stratified Turbulence', *Theoret. Comput. Fluid Dyn.* **2**, 279–290.
- Slingo, A.: 1990, 'Sensitivity of the Earth's Radiation Budget to Changes in Low Clouds', *Nature* **343**, 49–51.
- Smith, S. A. and Jonas, P. R.: 1995, 'Observations of the Turbulent Fluxes in Fields of Cumulus Clouds', *Quart. J. Roy. Meteorol. Soc.* **121**, 1185–1208.
- Stage, S. A. and Businger, J. A.: 1981a, 'A Model for Entrainment into a Cloud-Topped Marine Boundary Layer. Part I: Model Description and Application to a Cold-Air Outbreak Episode', *J. Atmos. Sci.* **38**, 2213–2229.
- Stage, S. A. and Businger, J. A.: 1981b, 'A Model for Entrainment into a Cloud-Topped Marine Boundary Layer. Part II: Discussion of Model Behaviour and Comparison with Other Models', *J. Atmos. Sci.* **38**, 2230–2242.
- Stevens, B., Cotton, W. R., Feingold, G., and Moeng, C.-H.: 1998, 'Large-Eddy Simulations of Strongly Precipitating, Shallow, Stratocumulus-Topped Boundary Layers', *J. Atmos. Sci.* **55**, 3616–3638.
- Tatang, M. A., Pan, W., Prinn, R. C., and MacRae, G. J.: 1997, 'An Efficient Method for Parametric Uncertainty Analysis of Numerical Geophysical Models', *J. Geophys. Res.* **102**, 21925–21932.

- Wang, S. and Wang, Q.: 1994, 'Roles of Drizzle in a One-Dimensional Third-Order Closure Model of Nocturnal Stratus-Topped Marine Boundary Layer', *J. Atmos. Sci.* **50**, 4022–4043.
- Wyngaard, J. C.: 1983, 'Lectures on the Planetary Boundary Layer', in D. K. Lilly and T. Gal-Chen (eds.), *Mesoscale Meteorology-Theories, Observations and Models*, Reidel, Dordrecht, pp. 603–650.
- Wyngaard, J. C., Coté, O. R., and Izumi, Y.: 1971, 'Local Free Convection, Similarity and the Budgets of Shear Stress and Heat Flux', *J. Atmos. Sci.* **28**, 1171–1182.

